Journal of Sound and Vibration 330 (2011) 1091–1110

Contents lists available at ScienceDirect

Journal of Sound and Vibration

journal homepage: www.elsevier.com/locate/jsvi

Parametric reduced-order models for predicting the vibration response of complex structures with component damage and uncertainties

Sung-Kwon Hong [a], Bogdan I. Epureanu [a,*], Matthew P. Castanier [b], David J. Gorsich [b]

[a] Department of Mechanical Engineering, University of Michigan, 2350 Hayward Street, Ann Arbor, MI 48109-2125, USA
[b] U.S. Army Tank Automotive Research, Development, and Engineering Center, Warren, MI 48397-5000, USA

ARTICLE INFO

Article history:
Received 4 March 2010
Received in revised form
22 September 2010
Accepted 22 September 2010
Handling Editor: H. Ouyang
Available online 18 November 2010

ABSTRACT

Modeling and fast reanalysis techniques are proposed for predicting the dynamic response of complex structures with uncertainty represented by parameter variability (in geometric and material properties) at component-level. The novel models allow for accurate reanalyses and are useful in many applications where the model of the pristine structure may not capture the changes in the system-level response due to component-level parameter variations. Herein, such models are obtained by using a novel approach based on a modified concept of component mode synthesis. The novel models, referred to as parametric reduced-order models, are developed for the general case of multiple substructures with parameter variabilities. Three types of parameteric variabilities are considered: (a) geometric (thickness) variability, (b) structural deformations (dents), and (c) cracks. For the first case, a novel parametrization of component-level mass and stiffness matrices is employed to predict the system-level response. For the second case, a novel approximate method based on static mode compensation is implemented. For the third case (cracks), a generalized formulation for the bi-linear frequency approximation is used. The predicted vibration responses of complex structures are shown to agree very well with results obtained using a much more computationally expensive commercial tool.

1. Introduction

Structural analyses based on finite element models (FEMs) are often used to predict vibration responses, stresses, and other structural characteristics to support design processes. Also, evaluating the effects of possible damages (such as cracks and dents) on the structural response is crucial in a wide variety of applications. As computing power increases, simulation techniques replace experiments for testing designs, especially when the experiments are considerably expensive or difficult to execute. However, the complexity of the designs can make the analysis very slow when many component changes are needed during the design process. This issue is particularly important because usual industrial FEMs (such as automobile bodies and complex airplane structural components) have millions of degrees of freedom (DOF). These detailed models, with very large numbers of DOF, have to be used to ensure high accuracy. However, the large computational cost

* Corresponding author. Tel.: +1 734 647 6391; fax: +1 734 764 4256.
E-mail addresses: sungkwon@umich.edu (S.-K. Hong), epureanu@umich.edu (B.I. Epureanu), matt.castanier@us.army.mil (M.P. Castanier), david.gorsich@us.army.mil (D.J. Gorsich).

0022-460X/$ - see front matter © 2010 Elsevier Ltd. All rights reserved.
doi:10.1016/j.jsv.2010.09.022

Nomenclature

BFA	bi-linear frequency approximation
CB-CMS	Craig–Bampton component mode synthesis
CMS	component mode synthesis
DOF	degrees of freedom
MC-PROM	multiple-component parametric reduced-order model
PROM	parametric reduced-order model
ROM	reduced-order model
SMC-CMS	component mode synthesis with static mode compensation

of direct analyses based on these large models detrimentally affects the design cycle, especially when it is necessary to evaluate the effects of parametric variability and damages on the structural response. Thus, model reduction techniques such as presented herein are necessary to reduce the computational cost.

An alternative to direct structural analysis of huge models is based on component mode synthesis. Many component mode synthesis-based reduced-order modeling techniques have been published [1–7] because component mode synthesis can be combined with a wide variety of FEM-based methods. In the context of vibration analysis, component mode synthesis is used by first dividing the global structure into components. Next, each component is projected onto a very small truncated set of (component-level) basis vectors that approximately span the space of the (component-level) response. As a result, the number of DOF required to model each component is considerably reduced compared to standard FEMs. Finally, the models of each component are assembled, and a global reduced-order model is synthesized. This last step can be performed in several ways. The most common approach is the fixed-interface Craig–Bampton component mode synthesis method [2]. Craig–Bampton component mode synthesis is well understood and frequently used because of its simplicity and numerical stability. Herein, Craig–Bampton component mode synthesis is used for the substructuring analysis.

Although many reduced-order models have been developed for structural analyses [8–13], they are not constructed for design or damage detection in complex structures. The key element that separates reduced-order models for design from the rest is that usual reduced-order models cannot easily be re-constructed when changes are applied (by design or through damage) in a few components of the overall system. Recently, design-oriented reduced-order models have been developed to avoid prohibitively expensive reanalyses of complex structures. These recent models are referred to as parametric reduced-order models. For example, Balmès and co-workers [14,15] calculated sets of modes for a few sample parameter values in the parameter space, and grouped them into a fixed augmented basis for the modes of the nominal system. This augmented basis was found to be suitable for a (parametric) family of models. However, the need for repeatedly solving many sample eigenproblems makes the approach impractical for global parametric reduced-order models of realistic industrial FEMs. To accelerate solving the sampled eigenproblems, this technique was combined with a component-based approach by Zhang and Park [16,17] for large FEMs. As a by-product, the eigenproblems of the sampled space are confined to one specific component, and the resulting global system is reduced substantially. However, in the projection phase, the component basis has to be expanded back into the global coordinates. Hence, the approach does not lead to true component-based parametric reduced-order models. To address that issue, substructural analysis techniques based on parametric reduced-order models have been developed [18]. However, those parametric reduced-order models can account for one parametric variability in one substructure only. In contrast, the new component parametric reduced-order models proposed herein allow several substructures to have parametric variability in characteristics such as geometric parameters (e.g. thickness), or material properties (e.g. Young's modulus). These new multiple-component parametric reduced-order models are obtained by managing the geometric compatibility conditions between substructures.

Geometric variations (e.g. dents in the structure, or thickness variability due to manufacturing) can be treated as parametric variability in the structure. Such an approach has been used for a few years for investigating the vibration of turbo-machinery bladed disks. For example, static mode compensation has been used for global models [19,20] to compute the vibration response of a structure which has dents or missing material. By accounting for the effects of geometric variability as though they are produced by external forces, a set of basis vectors can be established using a combination of normal modes of the pristine structure compensated by static modes. However, the static mode compensation method for geometric variations has not been applied for substructuring. Herein, component mode synthesis with static mode compensation is developed based on Craig–Bampton component mode synthesis. When substructures have dents, component mode synthesis with static mode compensation is applied to obtain the vibration response. Finally, the effects of parameter variations (e.g. thickness and geometric variations) are analyzed by multiple-component parametric reduced-order models and component mode synthesis with static mode compensation.

Typical FEM-based techniques for modeling cracks in complex structures lead to remarkably large models. Also, it is well known that system-level response characteristics (such as resonant frequencies) of cracked structures differ from their healthy counterparts. Hence, models which are accurate yet reduced-order are highly desirable for complex cracked structures. In general, a nonlinear analysis is needed to predict the vibration response of a cracked structure because the periodic opening and closing of the crack surfaces leads to a (piecewise linear) nonlinear response. For that, Poudou and Pierre [21,22] have developed a hybrid frequency–time domain method. In that method, the resonant frequencies of the cracked structure are found by a forced response analysis which is a nonlinear problem whose solution is complex and

computationally intensive. To alleviate this issue, the bi-linear frequency approximation (which was first used to predict resonant frequencies of single-DOF piecewise linear systems [23]) is generalized to large dimensional models. The approach herein builds on the early methods for studying the vibration of cracked beams and plates using a multi-DOF model. Chati et al. [24] have studied bi-linear frequency approximation for a two-dimensional cracked beam, and Saito et al. [25] have used bi-linear frequency approximation for a three-dimensional cracked plate. Note that the actual motion of the crack surfaces can be quite complex, and there may be more than two crack states (open and closed) when, for example, the crack closing proceeds gradually so that different regions of the crack surfaces close at different times. Although the generalized bi-linear frequency approximation cannot capture the effects of gradual opening and closing, it can provide approximate values for the resonant frequencies of complex cracked structures by employing linear analyses only. Also, the linear analyses required in bi-linear frequency approximation can be performed using Craig–Bampton component mode synthesis, and that further reduces the computational cost.

The key novel contributions of this paper are as follows. First, the proposed multiple-component parametric reduced-order models are developed for cases where parameter variations occur simultaneously in multiple components by developing a novel transformation matrix. Second, the static mode compensation approach is adapted for use with Craig–Bampton component mode synthesis to create a novel component-level analysis. Third, the geometric compatibility conditions normally used in Craig–Bampton component mode synthesis are generalized and adapted so that bi-linear frequency approximation can be implemented efficiently for crack analysis in conjunction with Craig–Bampton component mode synthesis, component mode synthesis with static mode compensation and multiple-component parametric reduced-order models.

This paper is organized as follows. In Section 2, bi-linear frequency approximation and Craig–Bampton component mode synthesis for the cracked structure are discussed. Also, multiple-component parametric reduced-order models for structures which have multiple components with parametric variability, and component mode synthesis with static mode compensation for components with geometric variations (such as dents) are formulated. Next, the models for all substructures are assembled by using an effective computational approach to implement geometric compatibility conditions. In Section 3, numerical simulations are used to demonstrate the proposed methods for an L-shape structure which has several substructures with thickness variation and also substructures with damage (dents). Also, bi-linear frequency approximation is implemented for a cracked L-shape structure. Next, the novel reduced-order modeling techniques are applied to a real vehicle model in Section 4. Finally, conclusions are summarized in Section 5.

2. Reduced-order modeling

2.1. Bi-linear frequency approximation and CB-CMS for cracked structures

Bi-linear systems are essentially nonlinear and the notions of natural frequencies and normal modes are, strictly speaking, not applicable. In this study we focus on the many cases where the forcing applied to the system is periodic and leads to a periodic response. Herein, the frequency corresponding to the response with the largest amplitude is referred to as a resonant response and its frequency is referred to as a resonant frequency. Note that the systems where penetration is allowed or the crack is considered closed are linear. In this work, we discuss a methodology to approximate the nonlinear resonant frequencies based on resonant frequencies of systems where penetration is allowed, or the crack is considered closed at all times. Herein, we consider bi-linear systems under harmonic excitation which are assumed to produce a periodic response. While periodic responses are certainly observed in many applications, they are not guaranteed to occur in all occasions. Even when periodic solutions are possible, there can be complicating features such as multiplicity of steady-state responses and dependency on initial conditions. Such cases are exciting but are beyond the scope of this work.

2.1.1. Bi-linear frequency approximation

In this section, the bi-linear frequency approximation (BFA) is generalized and used to analyze three-dimensional cracked structures. Initially, BFA was used to provide approximate resonant frequencies for single-DOF piecewise linear (bi-linear) systems. In essence, BFA can be expressed as [23]

$$\omega_b = \frac{2\omega_1\omega_2}{\omega_1+\omega_2}, \tag{1}$$

where ω_b is the approximate resonant frequency, ω_1 is the resonant frequency of one of the linear systems associated with the piecewise linear system, and ω_2 is that of the other linear system of the piecewise linear system. This expression is the exact solution for the undamped oscillation of a piecewise linear (bi-linear) single-DOF oscillator. The application of Eq. (1) is more complex for more general cases such as cracked plates because in those cases multiple DOF are located on the crack surfaces. Hence, the model involves multiple piecewise linear systems. Nevertheless, for many cases one can assume that the cracked system behaves as if it were defined by only two linear systems, corresponding to two states: one when the crack is fully open, and for when the crack fully is closed. In the following, these states are referred to as states 1 and 2.

The definition of the states 1 and 2 can be extended to those proposed by Chati et al. [24], who analyzed the in-plane bending vibrations of a cracked beam. Specifically, state 1 (open crack) is defined by removing the constraint of no penetration of the crack surfaces. That is, for state 1 there is no constraint applied on the relative motion between the

corresponding nodes (one on each crack surface) that are in contact when the crack is closed. Hence, for state 1, inter-penetration is allowed. Similarly, state 2 (closed crack) is defined by enforcing no penetration, but allowing sliding between the crack surfaces. That is, for state 2 the relative motion between the nodes (which are located on each of the two separate faces of the crack) is not allowed in the direction perpendicular to the crack surface. Their motion in the plane tangent to the crack surfaces is allowed. Hence, for state 2, sliding is allowed while inter-penetration is not allowed. The mathematical representation of these two states is detailed in Section 2.1.2.

2.1.2. CB-CMS for cracked structures

In this section, the fixed-interface Craig–Bampton CMS (CB-CMS) [2] method is used to construct reduced-order models (ROMs). This modeling approach is used because of its simplicity and computational stability. To apply CMS, the complex structure of interest is partitioned into substructures. The DOF of each substructure are further partitioned into active DOF on the interface (indicated by the superscript *A*), and omitted DOF in the interior (indicated by the superscript *O*). The mass and stiffness matrices for a component i can then be partitioned to obtain

$$\mathbf{M}_i = \begin{bmatrix} \mathbf{m}_i^{AA} & \mathbf{m}_i^{AO} \\ \mathbf{m}_i^{OA} & \mathbf{m}_i^{OO} \end{bmatrix} \quad \text{and} \quad \mathbf{K}_i = \begin{bmatrix} \mathbf{k}_i^{AA} & \mathbf{k}_i^{AO} \\ \mathbf{k}_i^{OA} & \mathbf{k}_i^{OO} \end{bmatrix}.$$

Next, the physical coordinates are changed to a set of coordinates representing the amplitudes of a selected set of fixed-interface component-level normal modes $\mathbf{\Phi}_i^N$ (indicated by the superscript *N*), and the amplitudes of the full set of static constraint modes $\mathbf{\Phi}_i^C = -\mathbf{k}_i^{OO^{-1}}\mathbf{k}_i^{OA}$ (indicated by the superscript *C*). The transformed mass and stiffness matrices for component i can be expressed as

$$\hat{\mathbf{M}}_i = \begin{bmatrix} \hat{\mathbf{m}}_i^{C} & \hat{\mathbf{m}}_i^{CN} \\ \hat{\mathbf{m}}_i^{NC} & \hat{\mathbf{m}}_i^{NN} \end{bmatrix} \quad \text{and} \quad \hat{\mathbf{K}}_i = \begin{bmatrix} \hat{\mathbf{k}}_i^{C} & \hat{\mathbf{k}}_i^{CN} \\ \hat{\mathbf{k}}_i^{NC} & \hat{\mathbf{k}}_i^{NN} \end{bmatrix}. \tag{2}$$

To model the dynamics of cracked structures and to apply BFA, the substructuring is done such that all cracks are along boundaries between adjacent substructures. Hence, all crack surfaces are boundaries between substructures. Thus, in Eq. (2), the DOF marked as *C* are obtained from interface DOF (which are the interface DOF for the ith substructure). The interface DOF are further divided into constraint DOF (shown by superscript *CC*) and free DOF (indicated by superscript *FF*) for BFA. For example, for state 1 (open crack), the DOF on the crack surfaces are completely free (and the inter-penetration of crack surfaces is allowed). These DOF on the crack surfaces (are free DOF for state 1 and) are indicated by superscript *FF* in Eq. (3). For state 2 (closed crack), sliding boundary conditions are applied at the crack surfaces as discussed in Section 2.1.1. Thus, the constrained DOF (for sliding boundary conditions) are denoted by superscript *CC* in Eq. (3). Using these two kinds of geometric compatibility conditions, the frequencies ω_1 and ω_2 in Eq. (1) are obtained through two separate linear analyses. Thus, if component i has a crack surface, the component-level mass and stiffness matrices are partitioned as

$$\hat{\mathbf{M}}_i = \begin{bmatrix} \hat{\mathbf{m}}_i^{CC} & \hat{\mathbf{m}}_i^{CF} & \hat{\mathbf{m}}_i^{CCN} \\ \hat{\mathbf{m}}_i^{FC} & \hat{\mathbf{m}}_i^{FF} & \hat{\mathbf{m}}_i^{FFN} \\ \hat{\mathbf{m}}_i^{NCC} & \hat{\mathbf{m}}_i^{NFF} & \hat{\mathbf{m}}_i^{NN} \end{bmatrix}$$

and

$$\hat{\mathbf{K}}_i = \begin{bmatrix} \hat{\mathbf{k}}_i^{CC} & \hat{\mathbf{k}}_i^{CF} & \hat{\mathbf{k}}_i^{CCN} \\ \hat{\mathbf{k}}_i^{FC} & \hat{\mathbf{k}}_i^{FF} & \hat{\mathbf{k}}_i^{FFN} \\ \hat{\mathbf{k}}_i^{NCC} & \hat{\mathbf{k}}_i^{NFF} & \hat{\mathbf{k}}_i^{NN} \end{bmatrix}. \tag{3}$$

The notation contains many superscripts such as *A*, *O*, *C*, *N*, *CC*, and *FF*. To clarify the meaning of these superscripts, Fig. 1 provides a conceptual view of the groups of DOFs corresponding to these superscripts. Since all crack surfaces are at interfaces between components, the geometric compatibility conditions at the interfaces between substructures are applied only for the DOF marked as *CC* in Eq. (3). For example, if a substructure does not have a crack surface, then there are no DOF marked as *FF*, and all DOF are marked as *CC*. Hence, the geometric compatibility conditions are applied to all DOF marked as *C* in Eq. (2). In general, all DOF on the boundaries are constrained *except* the DOF corresponding to the crack surfaces. The DOF along crack surfaces (denoted by *FF*) are not constrained. Also, note that all boundary DOF are active DOF, and the geometric compatibility conditions used to assemble every substructure are applied only to the DOF marked as *CC* in Eq. (3).

2.2. Multiple-component parametric reduced-order models

Global parametric reduced-order models (PROMs) [15] have been developed for fast reanalyses of structures with parametric variability in their properties. An important drawback of existing global PROMs is that they require computationally expensive calculations to determine multiple sets of system-level eigenvectors. These eigenvectors are

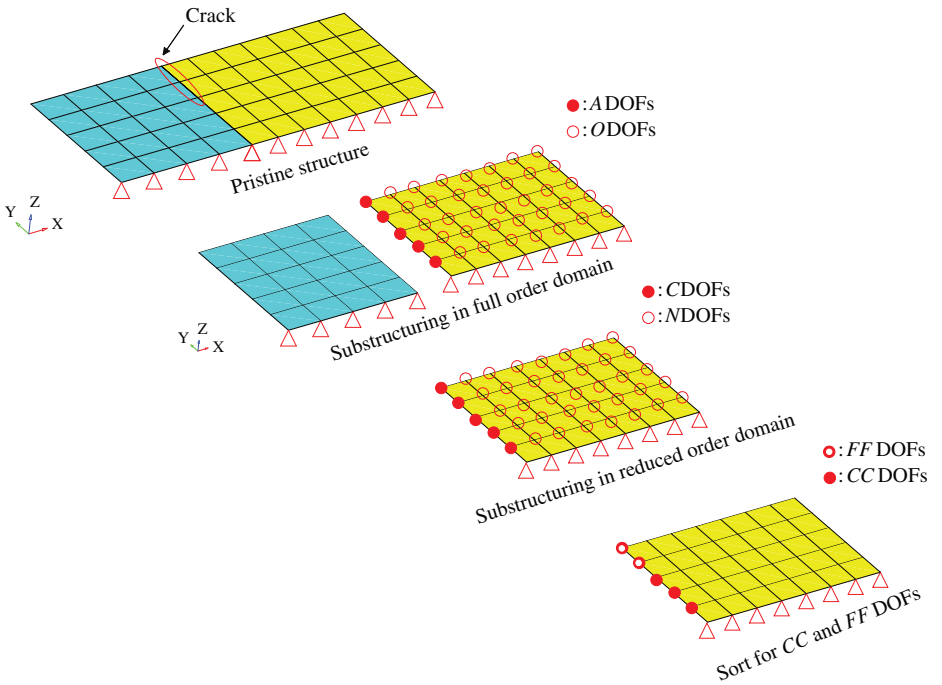

Fig. 1. Conceptual view of the groups of DOFs corresponding to superscripts *A*, *O*, *C*, *N*, *CC*, and *FF*.

needed when multiple parameters are considered. Thus, component-mode-based PROMs [16] have been developed to adopt component normal modes and characteristic constraint modes as projection basis instead of global modes. However, constructing component-mode-based PROMs is also time consuming because the approach still requires the calculation of system-level (global) interface modes. These interface modes are needed for the secondary modal analysis performed on the system-level matrix partitions (corresponding to the interface DOF) for all of the components in the global model. Thus, Park [18] introduced truly component-level analysis for constructing PROMs, referred to as component-PROMs. However, component-PROMs can be applied only to one component (and a single parametric variability). This issue is addressed herein by developing novel component-PROMs for multiple components. These new models can be used for cases where parametric variability (or damages) are present in several substructures simultaneously. For each substructure, a single variation is considered in parameters such as Young's modulus, or in geometric characteristics such as thickness. These models are referred to as multi-component PROMs (MC-PROMs).

A family of models can be defined as all models which differ only through a single parameter. Herein, we focus on families of component-level models first. Consider a family of models for parameter p for the ith component of a (global) structure. The mass and stiffness matrices of the ith component for this family of models can be approximated by using Taylor series. For example, for a linear thin plate element, the modification of the stiffness matrix due to variations in the thickness of the plate can be accurately represented by a Taylor series up to the third order, while the mass matrix can be approximated by a Taylor series up to first order, neglecting the rotary inertia [18]. The first and the third-order Taylor series approximations about the nominal parameter value p_0 can be expressed as follows:

$$\mathbf{M}_i(p) \approx \mathbf{M}_i(p_0) + \frac{\partial \mathbf{M}_i}{\partial p}(p-p_0),$$

$$\mathbf{K}_i(p) \approx \mathbf{K}_i(p_0) + \frac{\partial \mathbf{K}_i}{\partial p}(p-p_0) + \frac{1}{2}\frac{\partial^2 \mathbf{K}_i}{\partial p^2}(p-p_0)^2 + \frac{1}{6}\frac{\partial^3 \mathbf{K}_i}{\partial p^3}(p-p_0)^3. \tag{4}$$

Computationally, the partial derivatives in Eq. (4) can be approximated using standard finite differences for a small parameter variation Δp as follows:

$$\mathbf{M}^1_{\mathrm{FD}} = \frac{\partial \mathbf{M}_i}{\partial p} \approx \frac{\mathbf{M}_i(p_0+\Delta p) - \mathbf{M}_i(p_0)}{\Delta p},$$

$$\mathbf{K}^1_{\mathrm{FD}} = \frac{\partial \mathbf{K}_i}{\partial p} \approx \frac{\mathbf{K}_i(p_0+\Delta p) - \mathbf{K}_i(p_0)}{\Delta p},$$

$$\mathbf{K}_{\mathrm{FD}}^{2}=\frac{\partial^{2}\mathbf{K}_{i}}{\partial p^{2}}\approx\frac{1}{2}\frac{\mathbf{K}_{i}(p_{0}+\Delta p)-2\mathbf{K}_{i}(p_{0})+\mathbf{K}_{i}(p_{0}-\Delta p)}{\Delta p^{2}},$$

$$\mathbf{K}_{\mathrm{FD}}^{3}=\frac{\partial^{3}\mathbf{K}_{i}}{\partial p^{3}}\approx\frac{\mathbf{K}_{i}(p_{0}+2\Delta p)-3\mathbf{K}_{i}(p_{0}+\Delta p)+3\mathbf{K}_{i}(p_{0})-\mathbf{K}_{i}(p_{0}-\Delta p)}{\Delta p^{3}}. \tag{5}$$

Then, the parametrized component matrices can be obtained by substituting Eq. (5) into Eq. (4) to obtain

$$\mathbf{M}_{i}(p)\approx\mathbf{M}_{i}(p_{0})+\mathbf{M}_{\mathrm{FD}}^{1}(p-p_{0}),$$

$$\mathbf{K}_{i}(p)\approx\mathbf{K}_{i}(p_{0})+\mathbf{K}_{\mathrm{FD}}^{1}(p-p_{0})+\frac{1}{2}\mathbf{K}_{\mathrm{FD}}^{2}(p-p_{0})^{2}+\frac{1}{6}\mathbf{K}_{\mathrm{FD}}^{3}(p-p_{0})^{3}. \tag{6}$$

To obtain a ROM for a ith component, each parametric family of component models is projected onto a (constant) component-level modal basis $\hat{\mathbf{\Phi}}_i$. This basis is calculated (for each component) at a few given (perturbed) sets of parameter values. This basis is used for all configurations in the parameter space of the corresponding component. The component-level modal basis $\hat{\mathbf{\Phi}}_i$ for ith component can be expressed as

$$\hat{\mathbf{\Phi}}_{i}=\begin{bmatrix}\mathbf{I} & \mathbf{I} & \mathbf{0}\\ \mathbf{\Psi}_{i}^{0} & \mathbf{\Psi}_{i}^{U} & \mathbf{\Phi}_{i}^{\mathrm{aug}}\end{bmatrix}, \tag{7}$$

where $\mathbf{\Phi}_i^{\mathrm{aug}}$ is referred to as the matrix of augmented fixed-interface normal modes

$$\mathbf{\Phi}_{i}^{\mathrm{aug}}=[\mathbf{\Phi}_{i}^{0}\ \ \mathbf{\Phi}_{i}^{1}\ \ \mathbf{\Phi}_{i}^{2}\ \ \mathbf{\Phi}_{i}^{3}], \tag{8}$$

and the superscript 0 indicates quantities computed for the nominal parameter values, while the superscript U, 1, 2 and 3 indicate quantities computed for perturbed parameter values (which can be, for example, $p+\Delta p$, $p+2\Delta p$, and $p+3\Delta p$). Vectors $\mathbf{\Phi}_i$ and $\mathbf{\Psi}_i$ in Eq. (7) represent fixed-interface normal modes and static constraint modes.

When the stiffness matrix is represented by a third-order Taylor series, then the fixed-interface normal modes for three perturbed structures are computed to form a transformation matrix. In general, taken all together, the modes in $\mathbf{\Phi}_i^{\mathrm{aug}}$ are not orthogonal. For numerical stability, an orthogonal basis for the space spanned by these modes is used. To that aim, the left singular vectors of Eq. (8) are computed, and the left singular vector $\mathbf{U}$ corresponding to singular values larger than 0.01 percent of the maximum singular values are selected. Next, $\mathbf{U}$ is used to construct a transformation matrix (instead of the augmented fixed-interface normal modes $\mathbf{\Phi}_i^{\mathrm{aug}}$). The final transformation matrix can be expressed as

$$\hat{\mathbf{\Phi}}_{i}=\begin{bmatrix}\mathbf{I} & \mathbf{I} & \mathbf{0}\\ \mathbf{\Psi}_{i}^{0} & \mathbf{\Psi}_{i}^{U} & \mathbf{U}_{i}\end{bmatrix}, \tag{9}$$

Using Eq. (9) into Eq. (6), the physical coordinates are transformed to coordinates along the collected set of modes $\hat{\mathbf{\Phi}}_i$ for the ith component. The transformed mass and stiffness matrices can be expressed as

$$\hat{\mathbf{M}}_{i}(p)\approx\hat{\mathbf{\Phi}}_{i}^{\mathrm{T}}\mathbf{M}_{i}(p_{0})\hat{\mathbf{\Phi}}_{i}+\hat{\mathbf{\Phi}}_{i}^{\mathrm{T}}\mathbf{M}_{\mathrm{FD}}^{1}\hat{\mathbf{\Phi}}_{i}(p-p_{0}),$$

$$\hat{\mathbf{K}}_{i}(p)\approx\hat{\mathbf{\Phi}}_{i}^{\mathrm{T}}\mathbf{K}_{i}(p_{0})\hat{\mathbf{\Phi}}_{i}+\hat{\mathbf{\Phi}}_{i}^{\mathrm{T}}\mathbf{K}_{\mathrm{FD}}^{1}\hat{\mathbf{\Phi}}_{i}(p-p_{0})+\frac{1}{2}\hat{\mathbf{\Phi}}_{i}^{\mathrm{T}}\mathbf{K}_{\mathrm{FD}}^{2}\hat{\mathbf{\Phi}}_{i}(p-p_{0})^{2}+\frac{1}{6}\hat{\mathbf{\Phi}}_{i}^{\mathrm{T}}\mathbf{K}_{\mathrm{FD}}^{3}\hat{\mathbf{\Phi}}_{i}(p-p_{0})^{3}.$$

The modal basis consists of internal and interface DOF for each substructure. Thus, the mass and stiffness matrices for the ith component used for MC-PROM can be partitioned as follows:

$$\mathbf{M}_{i}^{\mathrm{PROM}}=\begin{bmatrix}\mathbf{m}_{i}^{C_{00}} & \mathbf{m}_{i}^{C_{0U}} & \mathbf{m}_{i}^{CN_{00}}\\ \mathbf{m}_{i}^{C_{U0}} & \mathbf{m}_{i}^{C_{UU}} & \mathbf{m}_{i}^{CN_{UU}}\\ \mathbf{m}_{i}^{NC_{00}} & \mathbf{m}_{i}^{NC_{UU}} & \mathbf{m}_{i}^{N_{d}}\end{bmatrix}, \tag{10}$$

$$\mathbf{K}_{i}^{\mathrm{PROM}}=\begin{bmatrix}\mathbf{k}_{i}^{C_{00}} & \mathbf{k}_{i}^{C_{0U}} & \mathbf{k}_{i}^{CN_{00}}\\ \mathbf{k}_{i}^{C_{U0}} & \mathbf{k}_{i}^{C_{UU}} & \mathbf{k}_{i}^{CN_{UU}}\\ \mathbf{k}_{i}^{NC_{00}} & \mathbf{k}_{i}^{NC_{UU}} & \mathbf{k}_{i}^{N_{d}}\end{bmatrix}. \tag{11}$$

In addition, the interface DOF are also divided into constrained DOF (denoted by superscript *CC*) and free DOF (denoted by superscript *FF*) to apply open and sliding boundary conditions for BFA as in Eq. (3). Thus, the interface DOF marked as *C* can also be divided into *CC* and *FF* DOF. Then, the MC-PROM mass and stiffness matrices can be

partitioned as

$$\mathbf{M}_i^{\mathrm{PROM}} = \begin{bmatrix} \mathbf{m}_i^{CC_{00}} & \mathbf{m}_i^{CF_{00}} & \mathbf{m}_i^{CC_{0U}} & \mathbf{m}_i^{CF_{0U}} & \mathbf{m}_i^{CCN_{00}} \\ \mathbf{m}_i^{FC_{00}} & \mathbf{m}_i^{FF_{00}} & \mathbf{m}_i^{FC_{0U}} & \mathbf{m}_i^{FF_{0U}} & \mathbf{m}_i^{FFN_{00}} \\ \mathbf{m}_i^{CC_{U0}} & \mathbf{m}_i^{CF_{U0}} & \mathbf{m}_i^{CC_{UU}} & \mathbf{m}_i^{CF_{UU}} & \mathbf{m}_i^{CCN_{UU}} \\ \mathbf{m}_i^{FC_{U0}} & \mathbf{m}_i^{FF_{U0}} & \mathbf{m}_i^{FC_{UU}} & \mathbf{m}_i^{FF_{UU}} & \mathbf{m}_i^{FFN_{UU}} \\ \mathbf{m}_i^{NCC_{00}} & \mathbf{m}_i^{NFF_{00}} & \mathbf{m}_i^{NCC_{UU}} & \mathbf{m}_i^{NFF_{UU}} & \mathbf{m}_i^{N_d} \end{bmatrix}, \tag{12}$$

$$\mathbf{K}_i^{\mathrm{PROM}} = \begin{bmatrix} \mathbf{k}_i^{CC_{00}} & \mathbf{k}_i^{CF_{00}} & \mathbf{k}_i^{CC_{0U}} & \mathbf{k}_i^{CF_{0U}} & \mathbf{k}_i^{CCN_{00}} \\ \mathbf{k}_i^{FC_{00}} & \mathbf{k}_i^{FF_{00}} & \mathbf{k}_i^{FC_{0U}} & \mathbf{k}_i^{FF_{0U}} & \mathbf{k}_i^{FFN_{00}} \\ \mathbf{k}_i^{CC_{U0}} & \mathbf{k}_i^{CF_{U0}} & \mathbf{k}_i^{CC_{UU}} & \mathbf{k}_i^{CF_{UU}} & \mathbf{k}_i^{CCN_{UU}} \\ \mathbf{k}_i^{FC_{U0}} & \mathbf{k}_i^{FF_{U0}} & \mathbf{k}_i^{FC_{UU}} & \mathbf{k}_i^{FF_{UU}} & \mathbf{k}_i^{FFN_{UU}} \\ \mathbf{k}_i^{NCC_{00}} & \mathbf{k}_i^{NFF_{00}} & \mathbf{k}_i^{NCC_{UU}} & \mathbf{k}_i^{NFF_{UU}} & \mathbf{k}_i^{N_d} \end{bmatrix}. \tag{13}$$

2.3. Component mode synthesis with static mode compensation

In this section, a novel, component-based modeling technique for systems containing dents is formulated using a mode-acceleration method based on static mode compensation (SMC). Lim et al. [20] used this modeling technique for structures with geometric variation. However, that SMC technique was applied to global structural analysis and not to substructural analysis. Herein, an SMC technique is developed for substructural analysis. The resulting reduced-order modeling method is referred to as component mode synthesis with static mode compensation (SMC-CMS). Note that, although this procedure is formally similar to CB-CMS, the bases used are distinct.

The mass and stiffness matrices of the ith dented substructure can be expressed as

$$\mathbf{M}_i^D = \begin{bmatrix} \mathbf{m}_i^{AA^D} \mathbf{m}_i^{AO^D} \\ \mathbf{m}_i^{OA^D} \mathbf{m}_i^{OO^D} \end{bmatrix} \quad \text{and} \quad \mathbf{K}_i^D = \begin{bmatrix} \mathbf{k}_i^{AA^D} \mathbf{k}_i^{AO^D} \\ \mathbf{k}_i^{OA^D} \mathbf{k}_i^{OO^D} \end{bmatrix},$$

where the DOF of each substructure have been partitioned into active DOF on the interface (indicated by the superscript A), and omitted DOF in the interior (indicated by the superscript O).

In the CB-CMS method, a selected set of fixed-interface component-level normal modes $\mathbf{\Phi}_i^N$ are obtained using the component-level mass and stiffness matrices $\mathbf{M}_i$ and $\mathbf{K}_i$. In contrast, in the SMC-CMS method, a truncated/selected set of fixed-interface normal modes calculated using SMC are used. Hence, the normal modes of the pristine/healthy substructure are compensated by using static modes. To that aim, the changes in the mass and stiffness matrices due to the presence of the dent are expressed as $\mathbf{M}_i^\delta = \mathbf{M}_i^D - \mathbf{M}_i^H$, and $\mathbf{K}_i^\delta = \mathbf{K}_i^D - \mathbf{K}_i^H$, where the superscripts D and H indicate dented and healthy substructures.

The active DOF (which are interface DOF between substructures) are needed for applying the geometric compatibility conditions. In addition to those DOF, there are other active DOF which have to be considered. These other active DOF (indicated by the subscript Γ) are DOF affected the dent. These DOF are needed to model the attachment modes used in the SMC-CMS method. The attachment modes $\mathbf{\Psi}^H$ are obtained using the DOF marked as Γ together with the omitted DOF.

One physical interpretation of SMC is that an equivalent force is applied to the structure to account for the changes in dynamics due to the dent. This equivalent force [19,20] can be expressed as

$$\mathbf{f}_{ij} = (-\omega_{ij}^{H^2} \mathbf{M}_i^{OO^D} + \mathbf{K}_i^{OO^D}) \mathbf{\Phi}_{ij}^H = \begin{bmatrix} \mathbf{0} \\ (-\omega_{ij}^{H^2} \mathbf{M}_i^{OO^\delta} + \mathbf{K}_i^{OO^\delta}) \mathbf{\Phi}_{\Gamma,ij}^H \end{bmatrix},$$

where ω_{ij}^H and $\mathbf{\Phi}_{ij}^H$ are the jth natural frequency and mode shape of the ith healthy substructure, and $\mathbf{\Phi}_{\Gamma,ij}^H$ are the portions of $\mathbf{\Phi}_{ij}^H$ which correspond to the DOF where a dent is present (i.e. the DOF marked as Γ). The static modes used in SMC are defined by $\mathbf{K}_i^{D^{-1}} \mathbf{f}_{ij}$, and can be obtained using the following relation [19,20]:

$$\mathbf{K}_i^{D^{-1}} \mathbf{f}_{ij} = \mathbf{K}_i^{H^{-1}} (\mathbf{I} + \mathbf{K}_i^\delta \mathbf{K}_i^{H^{-1}})^{-1} \mathbf{f}_{ij} = \mathbf{K}_i^{H^{-1}} \mathbf{g}_{ij}, \tag{14}$$

where

$$\mathbf{g}_{ij} = (\mathbf{I} + \mathbf{K}_i^\delta \mathbf{K}_i^{H^{-1}})^{-1} \mathbf{f}_{ij}.$$

Eq. (14) shows that the static modes can be obtained by a static analysis where the (static) forces $\mathbf{f}_{ij}$ are applied to the dented substructure, or the (static) forces $\mathbf{g}_{ij}$ are applied to the healthy substructure. Also, these static modes can be computed as a linear combination of healthy-structure attachment modes with the coefficients being the corresponding

forces, that is

$$\mathbf{K}^{D^{-1}}\mathbf{f}_{ij} = \mathbf{K}^{H^{-1}}\mathbf{g}_{ij} = \boldsymbol{\Psi}^{H}\mathbf{g}_{\Gamma,ij}.$$

Finally, the truncated set of component-level normal modes for the healthy substructure (compensated by static modes) can be obtained as

$$\boldsymbol{\Phi}_i^{\mathrm{SMC}} = \boldsymbol{\Phi}_i^{H} - \boldsymbol{\Psi}_i^{H}\mathbf{G}_{\Gamma,i}.$$

This set of modes is used in SMC-CMS to construct ROMs. The resulting ROMs are similar to the ones obtained using fixed-interface normal modes in CB-CMS.

Using the truncated set of normal modes $\boldsymbol{\Phi}_i^{\mathrm{SMC}}$, the reduced mass and stiffness matrices can be expressed as follows:

$$\mathbf{M}_i^{\mathrm{SMC}} = \begin{bmatrix} \mathbf{m}_i^{C} & \mathbf{m}_i^{C,SMC} \\ \mathbf{m}_i^{SMC,C} & \mathbf{m}_i^{\mathrm{SMC}} \end{bmatrix}, \tag{15}$$

$$\mathbf{K}_i^{\mathrm{SMC}} = \begin{bmatrix} \mathbf{k}_i^{C} & \mathbf{k}_i^{C,SMC} \\ \mathbf{k}_i^{SMC,C} & \mathbf{k}_i^{\mathrm{SMC}} \end{bmatrix}, \tag{16}$$

where the superscript C refers to constraint modes, and

$$\mathbf{m}_i^{C} = \mathbf{m}_i^{AA^D} + \boldsymbol{\Psi}_i^{C}\mathbf{m}_i^{OA^D} + \boldsymbol{\Psi}_i^{C^T}\mathbf{m}_i^{OO^D}\boldsymbol{\Psi}_i^{C^T},$$

$$\mathbf{m}_i^{C,SMC} = \mathbf{m}_i^{AO^D}\boldsymbol{\Phi}_i^{\mathrm{SMC}} + \boldsymbol{\Psi}_i^{C^T}\mathbf{m}_i^{OO^D}\boldsymbol{\Phi}_i^{\mathrm{SMC}},$$

$$\mathbf{m}_i^{SMC,C} = \mathbf{M}_i^{C,SMC^T},$$

$$\mathbf{m}_i^{\mathrm{SMC}} = \boldsymbol{\Phi}_i^{\mathrm{SMC}^T}\mathbf{m}_i^{OO^D}\boldsymbol{\Phi}_i^{\mathrm{SMC}},$$

$$\mathbf{k}_i^{C} = \mathbf{k}_i^{AA^D} + \boldsymbol{\Psi}_i^{C}\mathbf{k}_i^{OA^D} + \boldsymbol{\Psi}_i^{C^T}\mathbf{k}_i^{OO^D}\boldsymbol{\Psi}_i^{C^T},$$

$$\mathbf{k}_i^{C,SMC} = \mathbf{k}_i^{AO^D}\boldsymbol{\Phi}_i^{\mathrm{SMC}} + \boldsymbol{\Psi}_i^{C^T}\mathbf{k}_i^{OO^D}\boldsymbol{\Phi}_i^{\mathrm{SMC}},$$

$$\mathbf{k}_i^{SMC,C} = \mathbf{K}_i^{C,SMC^T},$$

$$\mathbf{k}_i^{\mathrm{SMC}} = \boldsymbol{\Phi}_i^{\mathrm{SMC}^T}\mathbf{k}_i^{OO^D}\boldsymbol{\Phi}_i^{\mathrm{SMC}}.$$

Similar to the CB-CMS and MC-PROM matrices used for BFA, the DOF marked as C can be partitioned into CC and FF DOF. One obtains

$$\mathbf{M}_j^{\mathrm{SMC}} = \begin{bmatrix} \mathbf{m}_j^{CC} & \mathbf{m}_j^{CF} & \mathbf{m}_j^{CC,\mathrm{SMC}} \\ \mathbf{m}_j^{FC} & \mathbf{m}_j^{FF} & \mathbf{m}_j^{FF,\mathrm{SMC}} \\ \mathbf{m}_j^{\mathrm{SMC},CC} & \mathbf{m}_j^{\mathrm{SMC},FF} & \mathbf{m}_j^{\mathrm{SMC}} \end{bmatrix}, \tag{17}$$

$$\mathbf{K}_j^{\mathrm{SMC}} = \begin{bmatrix} \mathbf{k}_j^{CC} & \mathbf{k}_j^{CF} & \mathbf{k}_j^{CC,\mathrm{SMC}} \\ \mathbf{k}_j^{FC} & \mathbf{k}_j^{FF} & \mathbf{k}_j^{FF,\mathrm{SMC}} \\ \mathbf{k}_j^{\mathrm{SMC},CC} & \mathbf{k}_j^{\mathrm{SMC},FF} & \mathbf{k}_j^{\mathrm{SMC}} \end{bmatrix}. \tag{18}$$

2.4. Geometric compatibility conditions for MC-PROM, CB-CMS and SMC-CMS

In MC-PROM, the component-level mass and stiffness matrices are spanned by matrices corresponding to the nominal and the perturbed parameters. Hence, the interface DOF (indicated by the superscript C) of the substructure are not the same in MC-PROM as in CB-CMS and SMC-CMS.

The component-level matrices used in CB-CMS and SMC-CMS (given in Eqs. (2), (15) and (16)) have single interface parts, so in this section, CMS indicates both CB-CMS and SMC-CMS. However, in Eqs. (10) and (11), one may note that the interface parts of

the PROM matrices are twice as many as those of the mass and stiffness matrices used in CB-CMS and SMC-CMS. Thus, geometric compatibility conditions are enforced to assemble these matrices (CB-CMS, SMC-CMS and MC-PROM), as described next.

Fig. 2 shows the procedure used to construct a PROM. In particular, reduced-order modeling techniques are applied to each substructure, and then geometric compatibility conditions are enforced. The process may be summarized as follows: (a) the system matrix is divided into components according to the type of parameter variation and/or damage, (b) a ROM is constructed for each substructure, (c) the constrained (*CC*) and free (*FF*) DOF are assigned for the substructures which have crack surfaces at their interface with other components, (d) substructures modelled using the CB-CMS or the SMC-CMS approach are assembled, (e) substructures modelled using the PROM approach are assembled, and (f) the partially assembled structure modelled using CB-CMS or SMC-CMS, and the partially assembled structure modelled using PROM are assembled together. Note that when each substructure is assembled, the geometric compatibility conditions are applied to the DOF marked as *CC*. A more detailed description of this procedure is as follows.

MC-PROM is applied for the design of the parts of the structure which have parametric variability, and CB-CMS is applied for the remainder of the structure. This remainder is the full structure minus the parametrized components (which are the components of interest in the design process, referred to as design components). In addition, SMC-CMS is applied for dented components.

Recall that the SMC-CMS method is similar to CB-CMS except that it uses a different truncated set of (component-level) normal modes. Hence, the interface parts for SMC-CMS and CB-CMS have the same meaning. Thus, dented components can be grouped together with the remainder of the structure for the purpose of applying geometric compatibility conditions.

In general, a complex structure has remainder substructures and substructures which have parameter variability. First, CB-CMS is applied for the nominal components, and SMC-CMS is applied for the dented components. Next, consider that a

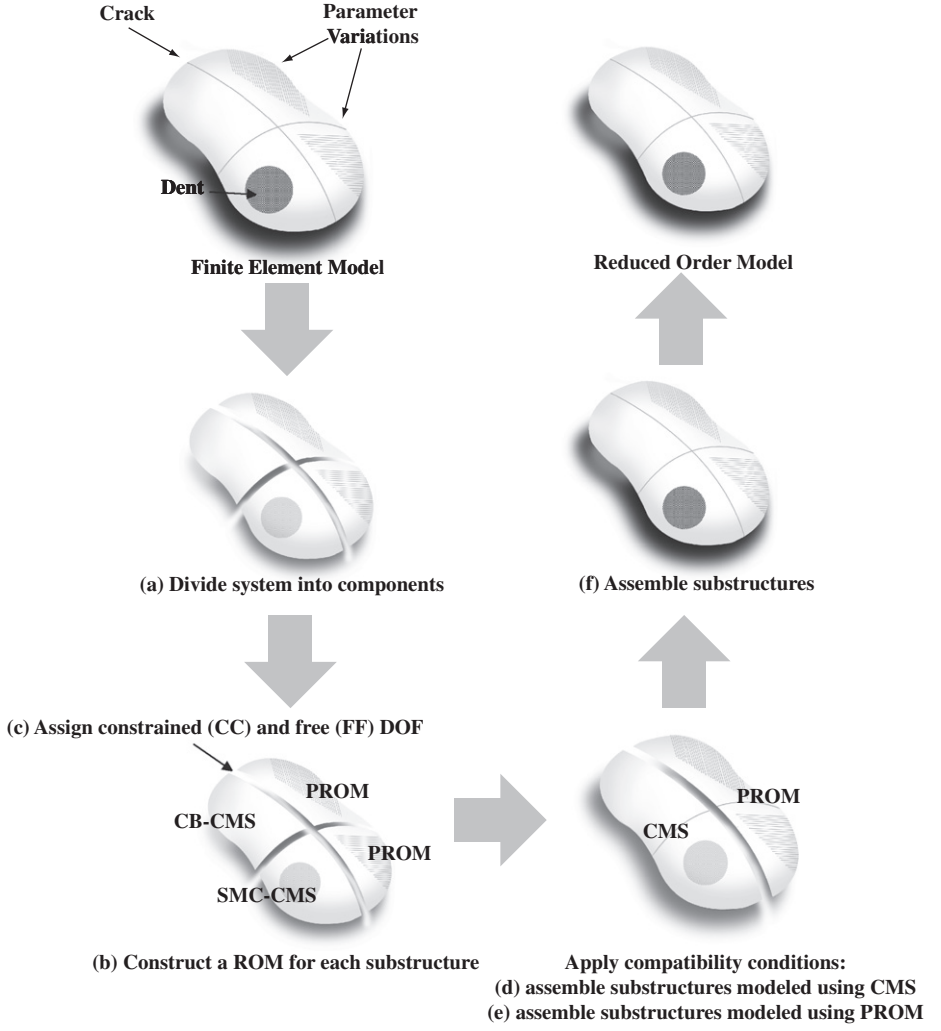

Fig. 2. Conceptual diagram depicting the process of building a PROM.

crack exists between substructure i (a reminder substructure where CMS is applied) and substructure j (a substructure which has parameter variability and where MC-PROM is applied). Then, the DOF marked as *FF* are assigned only for matrices of substructures i and j for the purpose of applying BFA. The complete, reduced-order, component-level equations of motion for each component based on CB-CMS, SMC-CMS and MC-PROM can be expressed as follows:

$$\mathbf{M}_i^{\mathrm{CMS}}\ddot{\mathbf{q}}_i^{\mathrm{CMS}}+\mathbf{K}_i^{\mathrm{CMS}}\mathbf{q}_i^{\mathrm{CMS}}=\mathbf{F}_i^{\mathrm{CMS}}\quad (i=1,2,\ldots),$$

$$\vdots$$

$$\mathbf{M}_j^{\mathrm{PROM}}\ddot{\mathbf{q}}_j^{\mathrm{PROM}}+\mathbf{K}_j^{\mathrm{PROM}}\mathbf{q}_j^{\mathrm{PROM}}=\mathbf{F}_j^{\mathrm{PROM}}\quad (j=1,2,\ldots).$$

To apply the interface compatibility conditions, the equations above are grouped into one global equation of motion. The resulting mass and stiffness matrices, and the forcing vector can be expressed as

$$\hat{\mathbf{M}}=\mathbf{Bdiag}[\mathbf{M}_1^{\mathrm{CMS}}\ \mathbf{M}_2^{\mathrm{CMS}}\ \cdots\ \mathbf{M}_1^{\mathrm{PROM}}\ \mathbf{M}_2^{\mathrm{PROM}}\ \cdots], \tag{19}$$

$$\hat{\mathbf{K}}=\mathbf{Bdiag}[\mathbf{K}_1^{\mathrm{CMS}}\ \mathbf{K}_2^{\mathrm{CMS}}\ \cdots\ \mathbf{K}_1^{\mathrm{PROM}}\ \mathbf{K}_2^{\mathrm{PROM}}\ \cdots], \tag{20}$$

$$\hat{\mathbf{F}}=[\mathbf{F}_1^{CMS\mathrm{T}}\ \mathbf{F}_2^{CMS\mathrm{T}}\ \cdots\ \mathbf{F}_1^{PROM\mathrm{T}}\ \mathbf{F}_2^{PROM\mathrm{T}}\ \cdots]^{\mathrm{T}}, \tag{21}$$

where **Bdiag**[·] denotes a block-diagonal matrix.

The first set of geometric compatibility conditions for CMS and MC-PROM are expressed (separately) as

$$\mathbf{q}^{CC_r}=\mathbf{q}_1^{CC_r}+\mathbf{q}_2^{CC_r}+\cdots,$$

$$\mathbf{q}^{CC_d00}=\mathbf{q}_1^{CC_d00}+\mathbf{q}_2^{CC_d00}+\cdots,$$

$$\mathbf{q}^{CC_dUU}=\mathbf{q}_1^{CC_dUU}+\mathbf{q}_2^{CC_dUU}+\cdots, \tag{22}$$

where the subscript r indicates components of the remainder of the structure, and the superscript 0 indicates quantities computed for the nominal parameter values, while the superscript U indicates quantities computed for perturbed parameter values (which can be, for example, the upper limits for the parameters of interest). Note that the geometric compatibility conditions are applied only for the constrained DOF.

Eq. (22) are applied into Eqs. (19)–(21) to assemble the matrices for CMS and MC-PROM, one part at a time. Then, these mass and stiffness matrices are assembled to obtain the full system-level matrices and forcing vector as

$$\overline{\hat{\mathbf{M}}}=\mathbf{Bdiag}[\mathbf{M}_{\mathrm{CMS}}\ \mathbf{M}_{\mathrm{PROM}}], \tag{23}$$

$$\overline{\hat{\mathbf{K}}}=\mathbf{Bdiag}[\mathbf{K}_{\mathrm{CMS}}\ \mathbf{K}_{\mathrm{PROM}}], \tag{24}$$

$$\overline{\hat{\mathbf{F}}}=[\mathbf{F}_{\mathrm{CMS}}^{\mathrm{T}}\ \mathbf{F}_{\mathrm{PROM}}^{\mathrm{T}}]^{\mathrm{T}}, \tag{25}$$

where

$$\mathbf{M}_{\mathrm{CMS}}=\begin{bmatrix}\mathbf{M}_{\mathrm{CMS}}^{CC_r} & \mathbf{M}_i^{CF_r} & \mathbf{M}_{\mathrm{CMS}}^{CCN_r}\\ \mathbf{M}_i^{FC_r} & \mathbf{M}_i^{FF_r} & \mathbf{M}_{\mathrm{CMS}}^{FFN_r}\\ \mathbf{M}_{\mathrm{CMS}}^{NCC_r} & \mathbf{M}_{\mathrm{CMS}}^{NFF_r} & \mathbf{M}_{\mathrm{CMS}}^{NN_r}\end{bmatrix},$$

$$\mathbf{K}_{\mathrm{CMS}}=\begin{bmatrix}\mathbf{K}_{\mathrm{CMS}}^{CC_r} & \mathbf{K}_j^{CF_r} & \mathbf{K}_{\mathrm{CMS}}^{CCN_r}\\ \mathbf{K}_j^{FC_r} & \mathbf{K}_j^{FF_r} & \mathbf{K}_{\mathrm{CMS}}^{FFN_r}\\ \mathbf{K}_{\mathrm{CMS}}^{NCC_r} & \mathbf{K}_{\mathrm{CMS}}^{NFF_r} & \mathbf{K}_{\mathrm{CMS}}^{NN_r}\end{bmatrix},\quad \mathbf{F}_{\mathrm{CMS}}=\begin{bmatrix}\mathbf{f}_1^{CC_r}+\mathbf{f}_2^{CC_r}+\cdots\\ \mathbf{f}_i^{FF_r}\\ \mathbf{f}_1^{NN_r}\\ \mathbf{f}_2^{NN_r}\\ \vdots\end{bmatrix},$$

$$\mathbf{M}_{\mathrm{PROM}}=\begin{bmatrix}\mathbf{M}_{\mathrm{PROM}}^{CC_{00}} & \mathbf{M}_{\mathrm{PROM}}^{CC_{0U}} & \mathbf{M}_j^{CF_{00}} & \mathbf{M}_j^{CF_{0U}} & \mathbf{M}_{\mathrm{PROM}}^{CCN_{00}}\\ \mathbf{M}_{\mathrm{PROM}}^{CC_{U0}} & \mathbf{M}_{\mathrm{PROM}}^{CC_{UU}} & \mathbf{M}_j^{CF_{UO}} & \mathbf{M}_j^{CF_{UU}} & \mathbf{M}_{\mathrm{PROM}}^{CCN_{UU}}\\ \mathbf{M}_{\mathrm{PROM}}^{FC_{00}} & \mathbf{M}_{\mathrm{PROM}}^{FC_{0U}} & \mathbf{M}_j^{FF_{00}} & \mathbf{M}_j^{FF_{0U}} & \mathbf{M}_{\mathrm{PROM}}^{FFN_{00}}\\ \mathbf{M}_{\mathrm{PROM}}^{FC_{U0}} & \mathbf{M}_{\mathrm{PROM}}^{FC_{UU}} & \mathbf{M}_j^{FF_{U0}} & \mathbf{M}_j^{FF_{UU}} & \mathbf{M}_{\mathrm{PROM}}^{FFN_{UU}}\\ \mathbf{M}_{\mathrm{PROM}}^{NCC_{00}} & \mathbf{M}_{\mathrm{PROM}}^{NCC_{UU}} & \mathbf{M}_j^{NFF_{00}} & \mathbf{M}_j^{NF_{UU}} & \mathbf{M}_{\mathrm{PROM}}^{NN_d}\end{bmatrix},$$

$$\mathbf{K}_{\mathrm{PROM}} = \begin{bmatrix} \mathbf{K}_{\mathrm{PROM}}^{CC_{00}} & \mathbf{K}_{\mathrm{PROM}}^{CC_{0U}} & \mathbf{K}_j^{CF_{00}} & \mathbf{K}_j^{CF_{0U}} & \mathbf{K}_{\mathrm{PROM}}^{CCN_{00}} \\ \mathbf{K}_{\mathrm{PROM}}^{CC_{U0}} & \mathbf{K}_{\mathrm{PROM}}^{CC_{UU}} & \mathbf{K}_j^{CF_{U0}} & \mathbf{K}_j^{CF_{UU}} & \mathbf{K}_{\mathrm{PROM}}^{CCN_{UU}} \\ \mathbf{K}_{\mathrm{PROM}}^{FC_{00}} & \mathbf{K}_{\mathrm{PROM}}^{FC_{0U}} & \mathbf{K}_j^{FF_{00}} & \mathbf{K}_j^{FF_{0U}} & \mathbf{K}_{\mathrm{PROM}}^{FFN_{00}} \\ \mathbf{K}_{\mathrm{PROM}}^{FC_{U0}} & \mathbf{K}_{\mathrm{PROM}}^{FC_{UU}} & \mathbf{K}_j^{FF_{U0}} & \mathbf{K}_j^{FF_{UU}} & \mathbf{K}_{\mathrm{PROM}}^{FFN_{UU}} \\ \mathbf{K}_{\mathrm{PROM}}^{NCC_{00}} & \mathbf{K}_{\mathrm{PROM}}^{NCC_{UU}} & \mathbf{K}_j^{NFF_{00}} & \mathbf{K}_j^{NF_{UU}} & \mathbf{K}_{\mathrm{PROM}}^{NN_d} \end{bmatrix},$$

$$\mathbf{F}_{\mathrm{PROM}} = \begin{bmatrix} \mathbf{f}_1^{CC_{00}} + \cdots + \mathbf{f}_N^{CC_{00}} \\ \mathbf{f}_1^{CC_{UU}} + \cdots + \mathbf{f}_N^{CC_{UU}} \\ \mathbf{f}_j^{FF_{00}} \\ \mathbf{f}_j^{FF_{UU}} \\ \mathbf{f}_1^{NN_d} \\ \mathbf{f}_2^{NN_d} \\ \vdots \end{bmatrix}.$$

Although the boundary DOF in the MC-PROM matrices are duplicated for the nominal and perturbed parameter parts, each relative displacement between DOF of adjacent substructures is still the same for CMS and MC-PROM. Therefore, a second set of geometric compatibility conditions is given by

$$\mathbf{q}_1^{CC_r} + \mathbf{q}_3^{CC_r} + \cdots + \mathbf{q}_L^{CC_r} = \mathbf{q}_2^{CC_{00}} + \mathbf{q}_2^{CC_{UU}} + \cdots + \mathbf{q}_N^{CC_{00}} + \mathbf{q}_N^{CC_{UU}}$$

or

$$\mathbf{q}^{CC_r} = \mathbf{q}^{CC_{00}} + \mathbf{q}^{CC_{UU}} = \mathbf{q}^{CC_d}.$$

By applying this second set of geometric compatibility conditions into Eqs. (23)–(25), the CMS and MC-PROM matrices and forcing vector can be rearranged to obtain the full system-level matrices as

$$\mathbf{M}_{\mathrm{sys}} = \begin{bmatrix} \mathbf{M}^{CC} & \mathbf{M}^{CF} & \mathbf{M}^{CCN} \\ \mathbf{M}^{FC} & \mathbf{M}^{FF} & \mathbf{M}^{FFN} \\ \mathbf{M}^{NCC} & \mathbf{M}^{NFF} & \mathbf{M}^{NN} \end{bmatrix}, \tag{26}$$

$$\mathbf{K}_{\mathrm{sys}} = \begin{bmatrix} \mathbf{K}^{CC} & \mathbf{K}^{CF} & \mathbf{K}^{CCN} \\ \mathbf{K}^{FC} & \mathbf{K}^{FF} & \mathbf{K}^{FFN} \\ \mathbf{K}^{NCC} & \mathbf{K}^{NFF} & \mathbf{K}^{NN} \end{bmatrix}, \tag{27}$$

$$\mathbf{F}_{\mathrm{sys}} = \begin{bmatrix} \mathbf{f}^{CC} \\ \mathbf{f}^{FF} \\ \mathbf{f}^{NN} \end{bmatrix}, \tag{28}$$

where

$$\mathbf{M}^{CC} = \begin{bmatrix} \mathbf{M}_{00}^{CC} & \mathbf{M}_{0U}^{CC} \\ \mathbf{M}_{U0}^{CC} & \mathbf{M}_{UU}^{CC} \end{bmatrix},$$

$$\mathbf{M}^{CF} = \begin{bmatrix} \mathbf{M}_i^{CF} & \mathbf{M}_j^{CF_{00}} & \mathbf{M}_j^{CF_{0U}} \\ \mathbf{M}_i^{CF} & \mathbf{M}_j^{CF_{U0}} & \mathbf{M}_j^{CF_{UU}} \end{bmatrix},$$

$$\mathbf{M}^{CCN} = \begin{bmatrix} \mathbf{m}_1^{C_rN_r} & \mathbf{m}_2^{C_rN_r} & \cdots & \mathbf{m}_1^{C_0N_d} & \mathbf{m}_2^{C_0N_d} & \cdots \\ \mathbf{m}_1^{C_rN_r} & \mathbf{m}_2^{C_rN_r} & \cdots & \mathbf{m}_1^{C_UN_d} & \mathbf{m}_2^{C_UN_d} & \cdots \end{bmatrix},$$

$$\mathbf{M}^{FC} = \mathbf{M}^{CF\mathrm{T}},$$

$$\mathbf{M}^{FF} = \begin{bmatrix} \mathbf{M}_i^{FF} & \mathbf{0} & \mathbf{0} \\ \mathbf{0} & \mathbf{M}_j^{FF_{00}} & \mathbf{M}_j^{FF_{0U}} \\ \mathbf{0} & \mathbf{M}_j^{FF_{0U}} & \mathbf{M}_j^{FF_{UU}} \end{bmatrix},$$

$$\mathbf{M}^{FFN}=\begin{bmatrix}\mathbf{m}_i^{FFN_r} & \mathbf{0} & \cdots & \mathbf{0} & \mathbf{0} & \cdots & \mathbf{0}\\ \mathbf{0} & \mathbf{0} & \cdots & \mathbf{0} & \mathbf{M}_j^{FFN_{00}} & \cdots & \mathbf{0}\\ \mathbf{0} & \mathbf{0} & \cdots & \mathbf{0} & \mathbf{M}_j^{FFN_{UU}} & \cdots & \mathbf{0}\end{bmatrix},$$

$$\mathbf{M}^{NCC}=\mathbf{M}^{CCN^{\mathrm{T}}},\quad \mathbf{M}^{NFF}=\mathbf{M}^{FFN^{\mathrm{T}}},$$

$$\mathbf{M}^{N}=\begin{bmatrix}\mathbf{m}_1^{NN_r} & \mathbf{0} & \mathbf{0} & \mathbf{0} & \mathbf{0} & \mathbf{0}\\ \mathbf{0} & \mathbf{m}_2^{NN_r} & \mathbf{0} & \mathbf{0} & \mathbf{0} & \mathbf{0}\\ \mathbf{0} & \mathbf{0} & \ddots & \mathbf{0} & \mathbf{0} & \mathbf{0}\\ \mathbf{0} & \mathbf{0} & \mathbf{0} & \mathbf{m}_1^{NN_d} & \mathbf{0} & \mathbf{0}\\ \mathbf{0} & \mathbf{0} & \mathbf{0} & \mathbf{0} & \mathbf{m}_2^{NN_d} & \mathbf{0}\\ \mathbf{0} & \mathbf{0} & \mathbf{0} & \mathbf{0} & \mathbf{0} & \ddots\end{bmatrix},$$

$$\mathbf{K}^{CC}=\begin{bmatrix}\mathbf{K}_{00}^{CC} & \mathbf{K}_{0U}^{CC}\\ \mathbf{K}_{U0}^{CC} & \mathbf{K}_{UU}^{CC}\end{bmatrix},$$

$$\mathbf{K}^{CF}=\begin{bmatrix}\mathbf{K}_i^{CF} & \mathbf{K}_j^{CF_{00}} & \mathbf{K}_j^{CF_{0U}}\\ \mathbf{K}_i^{CF} & \mathbf{K}_j^{CF_{U0}} & \mathbf{K}_j^{CF_{UU}}\end{bmatrix},$$

$$\mathbf{K}^{CCN}=\begin{bmatrix}\mathbf{k}_1^{C_rN_r} & \mathbf{k}_2^{C_rN_r} & \cdots & \mathbf{k}_1^{C_0N_d} & \mathbf{k}_2^{C_0N_d} & \cdots\\ \mathbf{k}_1^{C_rN_r} & \mathbf{k}_2^{C_rN_r} & \cdots & \mathbf{k}_1^{C_UN_d} & \mathbf{k}_2^{C_UN_d} & \cdots\end{bmatrix},$$

$$\mathbf{K}^{FC}=\mathbf{K}^{CF^{\mathrm{T}}},$$

$$\mathbf{K}^{FF}=\begin{bmatrix}\mathbf{K}_i^{FF} & \mathbf{0} & \mathbf{0}\\ \mathbf{0} & \mathbf{K}_j^{FF_{00}} & \mathbf{K}_j^{FF_{0U}}\\ \mathbf{0} & \mathbf{K}_j^{FF_{0U}} & \mathbf{K}_j^{FF_{UU}}\end{bmatrix},$$

$$\mathbf{K}^{FFN}=\begin{bmatrix}\mathbf{k}_i^{FFN_r} & \mathbf{0} & \cdots & \mathbf{0} & \mathbf{0} & \cdots & \mathbf{0}\\ \mathbf{0} & \mathbf{0} & \cdots & \mathbf{0} & \mathbf{K}_j^{FFN_{00}} & \cdots & \mathbf{0}\\ \mathbf{0} & \mathbf{0} & \cdots & \mathbf{0} & \mathbf{K}_j^{FFN_{UU}} & \cdots & \mathbf{0}\end{bmatrix},$$

$$\mathbf{K}^{NCC}=\mathbf{K}^{CCN^{\mathrm{T}}},\quad \mathbf{K}^{NFF}=\mathbf{K}^{FFN^{\mathrm{T}}},$$

$$\mathbf{K}^{N}=\begin{bmatrix}\mathbf{k}_1^{NN_r} & \mathbf{0} & \mathbf{0} & \mathbf{0} & \mathbf{0} & \mathbf{0}\\ \mathbf{0} & \mathbf{k}_2^{NN_r} & \mathbf{0} & \mathbf{0} & \mathbf{0} & \mathbf{0}\\ \mathbf{0} & \mathbf{0} & \ddots & \mathbf{0} & \mathbf{0} & \mathbf{0}\\ \mathbf{0} & \mathbf{0} & \mathbf{0} & \mathbf{k}_1^{NN_d} & \mathbf{0} & \mathbf{0}\\ \mathbf{0} & \mathbf{0} & \mathbf{0} & \mathbf{0} & \mathbf{k}_2^{NN_d} & \mathbf{0}\\ \mathbf{0} & \mathbf{0} & \mathbf{0} & \mathbf{0} & \mathbf{0} & \ddots\end{bmatrix},$$

$$\mathbf{F}^{CC}=\begin{bmatrix}\mathbf{f}_1^{CC_r}+\mathbf{f}_2^{CC_r}+\cdots+\mathbf{f}_1^{CC_0}+\mathbf{f}_2^{CC_0}+\cdots\\ \mathbf{f}_1^{CC_r}+\mathbf{f}_2^{CC_r}+\cdots+\mathbf{f}_1^{CC_U}+\mathbf{f}_2^{CC_U}+\cdots\end{bmatrix},$$

$$\mathbf{F}^{FF}=\begin{bmatrix}\mathbf{f}_i^{FF}\\ \mathbf{f}_j^{FF_{00}}\\ \mathbf{f}_j^{FF_{UU}}\end{bmatrix}\quad\text{and}\quad \mathbf{F}^{NN}=\begin{bmatrix}\mathbf{f}_1^{NN_r}\\ \mathbf{f}_2^{NN_r}\\ \vdots\\ \mathbf{f}_1^{NN_d}\\ \mathbf{f}_2^{NN_d}\\ \vdots\end{bmatrix}.$$

Eqs. (26)–(28) represent the assembled system matrices and forcing vector for the global ROM. However, the system matrices are (in general) singular due to the transformation matrix used for PROM in Eq. (9). There, the constraint modes Ψ_i^0 for the nominal parameter values (indicated by superscript 0) and the constraint modes Ψ_i^U for a perturbed parameter value can be linearly dependent. Thus, to numerically stabilize the system, the modal assurance criterion (MAC) for Ψ_i^0 and Ψ_i^U is used when the ith component PROM matrices are obtained. The MAC is given by

$$\mathbf{MAC}_i = \frac{\Psi_i^{0T}\Psi_i^U}{\sqrt{\Psi_i^{0T}\Psi_i^0}\sqrt{\Psi_i^{UT}\Psi_i^U}}, \quad \mathbf{e}_{jj}^i(\mathbf{MAC}_i) = \begin{cases} 0 & \text{MAC} \geq \varepsilon, \\ 1 & \text{MAC} < \varepsilon, \end{cases}$$

where subscript j in e_{jj} indicates the jth static constraint mode, and ε is a constant close to 1 which is used to distinguish linearly dependent modes among all the static constraint modes. Note that only the counterpart modes for the perturbed parameter case need to be checked against those of the nominal parameter case. Here, $\mathbf{e}_{jj}^i$ is a vector used to decide whether to keep or to eliminate the static constraint mode j of the PROM substructure i. The entries of the eliminating vector consist only of 0 or 1. Using the eliminating vector $\mathbf{e}_{jj}^i$, the system matrices are reduced by eliminating DOF which correspond to the perturbed parameter case.

3. Results for a moderately complex structure: L-shape structure

To demonstrate the proposed MC-PROM, SMC-CMS and BFA methodologies, an L-shaped structure (shown in Fig. 3) with various parameter variations and dents has been investigated numerically. The left side of Fig. 3 is the pristine structure, and the right side of Fig. 3 shows the damaged structure. The forced response of the L-shape structure is computed, and resonant frequencies are identified. The structure consists of eight substructures. Substructures 1, 6 and 7 have thickness variations as shown by cases 1 and 2 in Table 1. Moreover, substructures 3 and 5 have geometric variations (dents). The CB-CMS method is applied for the remainder of the structure (the part of the structure which does not have any thickness or other geometric variations). Those are substructures 2, 4, and 8. The remainder substructures are healthy and have nominal thickness of 0.4 mm. The MC-PROM and SMC-CMS methods are implemented for thickness and geometric variations, respectively.

Fig. 4 shows the system-level forced response for the healthy structure and the two cases of thickness variation. The response predicted by the PROM agrees well with the response proved by the full order model. On the left in Fig. 4, the dotted line represents the vibration response for the healthy structure, and the solid line is the response of the damaged structure with thickness variation (case 1) and dents. Both these results are obtained using a full finite element model and response calculations performed using NASTRAN. Also, NASTRAN was used to obtain the finite element mass and stiffness

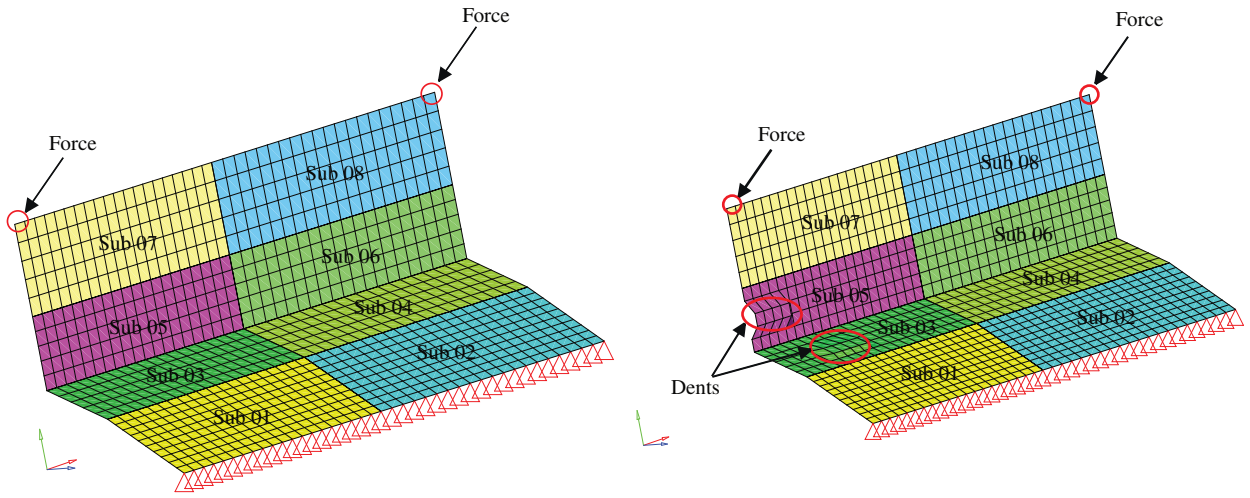

Fig. 3. Healthy structure and damaged structure with thickness variations.

Table 1
Thickness variations in substructures 1, 6 and 7.

Substructure	Thickness, case 1	Thickness, case 2
1	0.4 mm → 0.473 mm	0.4 mm → 0.435 mm
6	0.4 mm → 0.422 mm	0.4 mm → 0.491 mm
7	0.4 mm → 0.493 mm	0.4 mm → 0.481 mm

Table 2
Comparison of the full order model and the PROM.

Types	Full order model	PROM
System DOF	119,808	2420
Initial analysis time (s)	60,125	21,955
Reanalyses time (s)	60,125	595

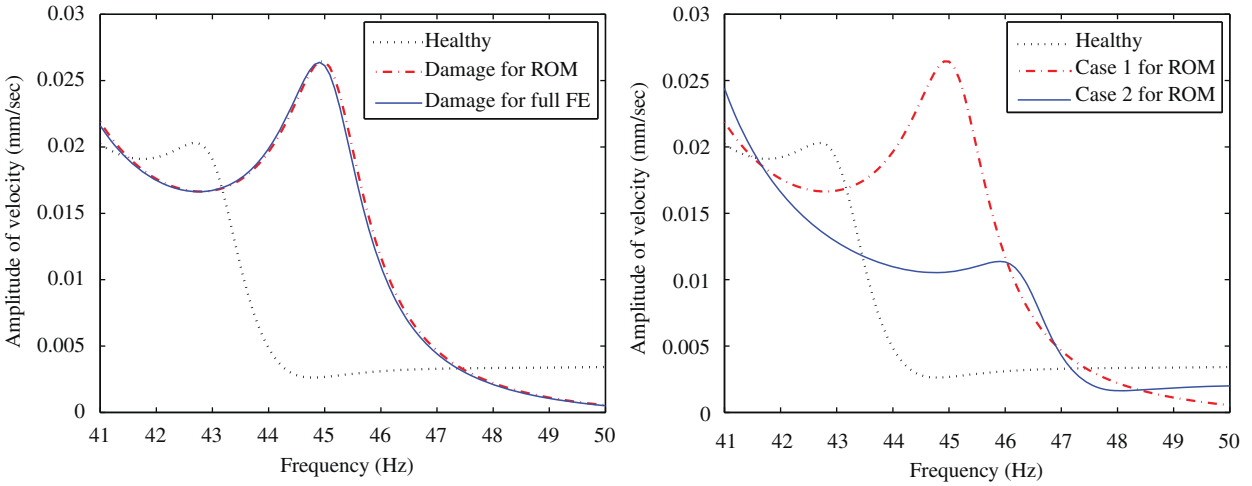

Fig. 4. Forced response predictions provided by a full finite element model and a PROM for the healthy and damaged structures with thickness variations for cases 1 and 2.

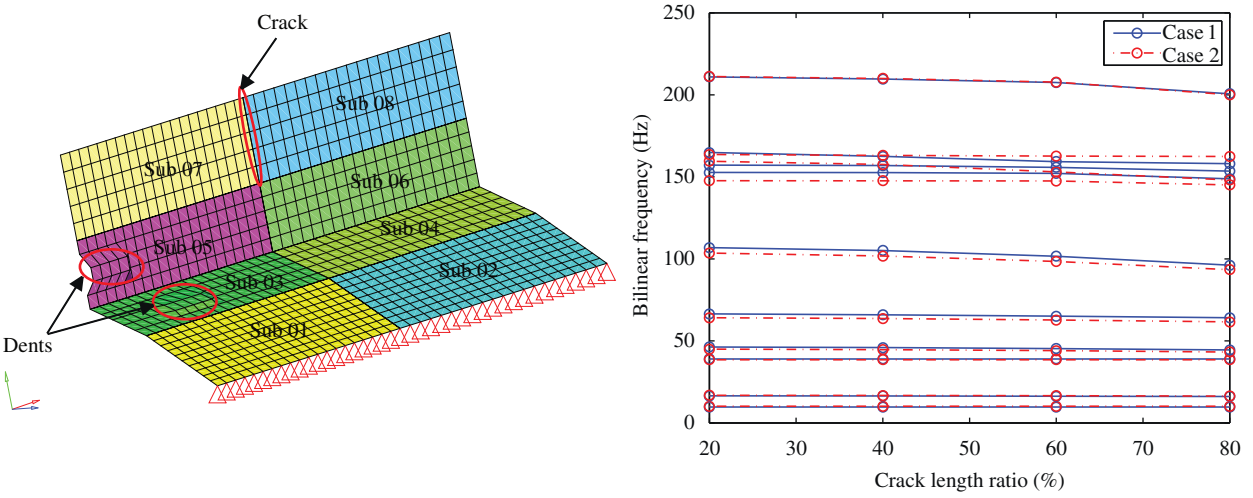

Fig. 5. Cracked structure with geometric and thickness variations, and resonant frequencies predicted using BFA for the first 10 modes.

matrices and force vectors. Using that information from NASTRAN, an in-house code was used to compute the structural vibration response.

The dashed line shows results obtained using a PROM based on CB-CMS, SMC-CMS, and MC-PROM. The results provided by the full model agree very well with those obtained using the novel PROM. In addition, on the right in Fig. 4, the dotted line is the response of the healthy structure, and the dashed line and the solid line are those for cases 1 and 2, respectively. These results show that the example considered is a challenging one because even small structural variations in one component affect the system-level vibration response.

The left side of Fig. 5 shows the structure which has not only a dent and thickness variations as in cases 1 and 2, but also a crack between substructures 7 and 8. This structure has the same dents and thickness variations as in cases 1 and 2. The resonant frequencies of the first 10 modes are shown on the right in Fig. 5. The solid line and the dashed line are the

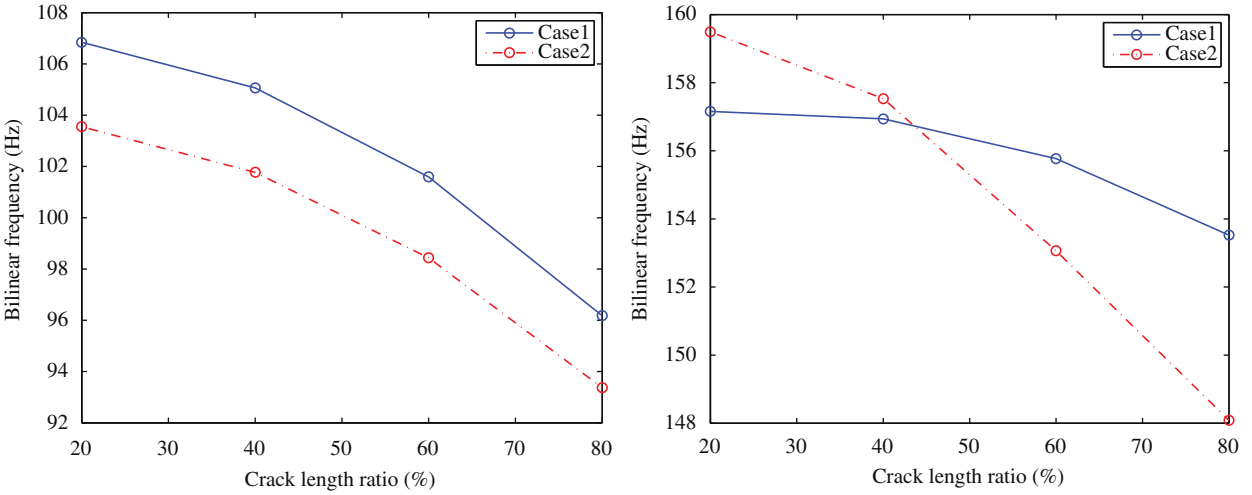

Fig. 6. Shifts of resonant frequencies for cases 1 and 2 for the 6th and 8th modes.

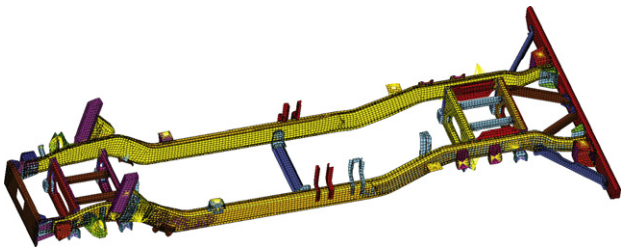

Fig. 7. HMMWV frame FE model.

resonant frequencies for cases 1 and 2, respectively. The right side of Fig. 5 shows that the frequencies of the higher modes are shifted (compared to the healthy structure) more than frequencies of the lower modes. Fig. 6 shows the shift of the resonant frequency for the 6th and 8th modes, respectively. The crack length varies from 20 to 80 percent (of structure's width). Note that the resonant frequencies are also shifted due to the thickness variations.

4. Results for a complex structure: HMMWV frame

In Section 3, the PROM method is applied to a moderately large model which consists of eight substructures. The total number of DOF of the L-shape structure is not huge, so the analysis time using the full order and reduced-order models are not dramatically different. In this section, the PROM method is used to predict the dynamic response of a realistic vehicle model which is the base frame of a high mobility multipurpose wheeled vehicle (HMMWV). The finite element model for the HMMWV is a conventional model used to examine its dynamic response. Fig. 7 shows the finite element model of the HMMWV frame, and Fig. 8 shows each substructure of the HMMWV frame for constructing a PROM. The substructure which represents the reinforcement frame of the back and front left-rails have thickness variations, and the engine cradle has a dent. Table 3 shows two cases of thickness variation of the reinforcement frames. The total number of DOF of the HMMWV model is 119,808, and the calculation time for one full order analysis takes more than 6 h. However, the PROM approach reduces the number of DOF of the system and lowers the calculation time dramatically. Not only the time needed for the initial calculation is shortened, but also the time for subsequent analyses is drastically decreased.

In Table 2, the number of DOF and the computational time required for the initial analysis and for the reanalyses are shown. The number of DOF of the PROM is much lower than that for the full order finite element model. Note that natural frequencies are needed for BFA. If natural frequencies are obtained from the full order finite element model which has 119,808 DOF, the calculation time is much longer than that required by PROM because PROM requires fewer than 2000 DOF. In addition, the initial analysis time needed for the PROM approach is 3 times shorter than that required by the full order finite element model. Also, the reanalysis time is 100 times faster than the time required by the full order finite element model. The time savings are not as large for the initial analysis as they are for reanalyses because of the need for an eigenanalysis to form the transformation matrix for each damage type.

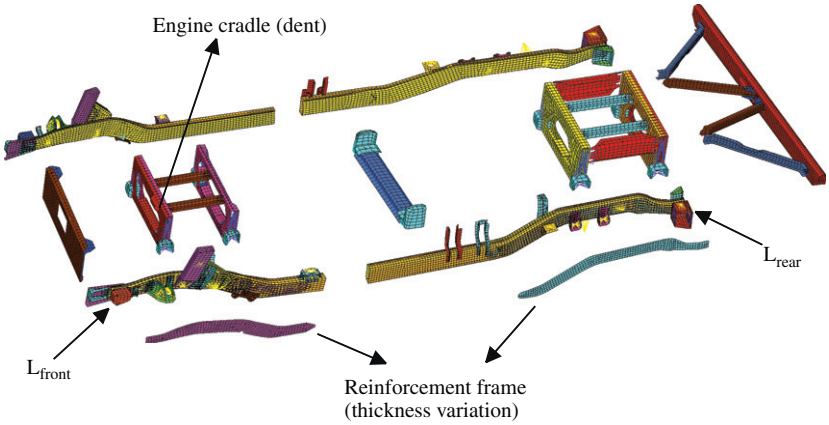

Fig. 8. Substructuring for HMMWV frame.

Table 3
Thickness variations for the HMMWV frame in substructures L_{front} and L_{rear}.

Substructure	Thickness, case 1	Thickness, case 2
L_{front}	3.0378 mm→4.6268 mm	3.0378 mm→5.5788 mm
L_{rear}	3.0378 mm→5.3838 mm	3.0378 mm→4.0908 mm

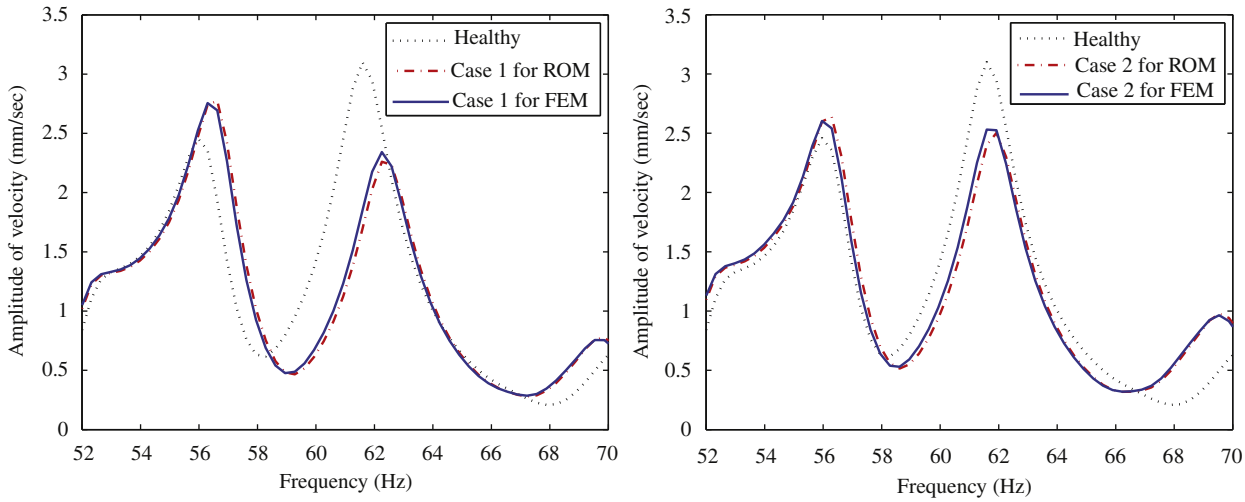

Fig. 9. Forced response predictions provided by a full finite element model and a PROM for the healthy and damaged structures with thickness variations for cases 1 and 2 of the HMMWV frame.

Next, forces and moments are applied as excitations in several nodal points of the structure. Force and moments can be applied by the tires, the engine, and several other external factors such as the aerodynamics. Herein, forces and moments from the engine are considered. Fig. 9 shows the response of the HMMWV frame for cases 1 and 2 of thickness variation, respectively. The dotted line shows the forced response of the healthy HMMWV structure, and the dashed line and the solid line show the response of the damaged HMMWV frame. Results obtained using a PROM and the full order model are shown.

Fig. 10 shows the finite element model of the cracked cross frame for the HMMWV frame. The crack length varies across the frame component from 11.11 to 88.89 percent. BFA is used to compute the resonant frequencies of the cracked HMMWV frame model. Note that the other damages (such as dents and thickness variations) are as in the cases 1 and 2. The resonant frequencies for cases 1 and 2 of thickness variation of the cracked and dented HMMWV frame model are shown in Figs. 11–13. These figures show the modes from the 1st mode to the 5th mode, the 11th mode to the 15th mode, and the 26th mode to the 30th mode, respectively. The lower frequencies shown in Fig. 11 do not shift much as the crack

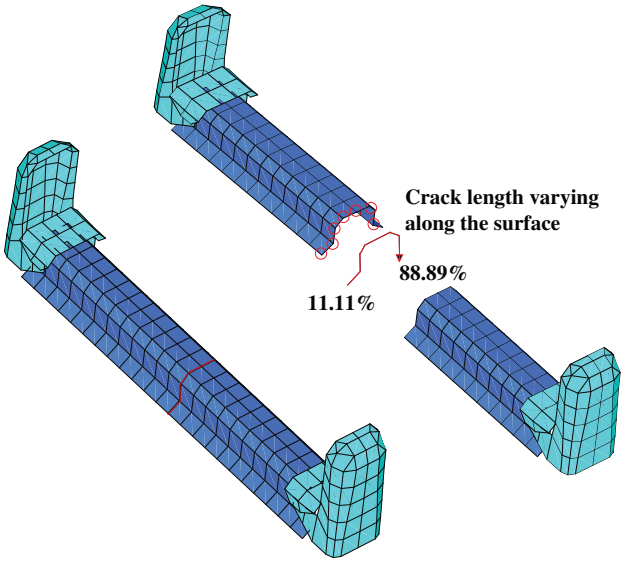

Fig. 10. Cracked base frame component.

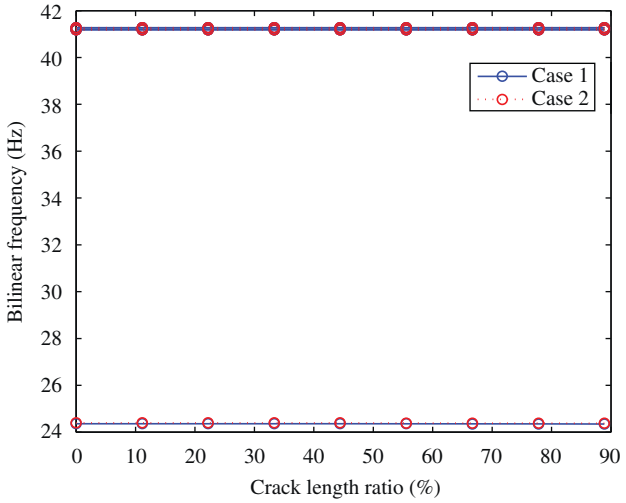

Fig. 11. Resonant frequencies predicted using BFA for the first 5 modes.

length increases. However, the mid-range resonant frequencies shift much more as the crack length increases, as shown in Fig. 12. Note that several modes switch when the crack length is around 40 percent. For the higher modes shown in Fig. 13, the frequencies shift more than those in Fig. 11, but the mode switching does not take place. Figs. 14 and 15 show the 14th and 25th resonant frequency of the cracked and dented HMMWV frame for cases 1 and 2 of thickness variations. These figures show that the resonant frequencies decrease significantly, once the crack length is larger than about 60 percent.

5. Conclusions and discussion

Novel multiple-component parametric reduced-order models (MC-PROMs) for predicting the vibration response of complex structures have been developed. These models are able to handle simultaneously with very high efficiency both parametric variability in multiple components as well as damage. Also, the parametric reduced-order models (PROMs) developed are agile and easy to construct, which makes them particularly useful for analyses required in design processes.

In addition, the reanalysis time for parametric reduced-order models (PROM) is significantly shorter than that for the full order model. For example, to perform reanalyses which account for thickness variations (such as the ones in case 2 for the high mobility multipurpose wheeled vehicle (HMMWV) model) or new types of dents, the parametric reduced-order models (PROM) approach needs only a few simple matrix calculations (without the need for eigenanalyses) to construct

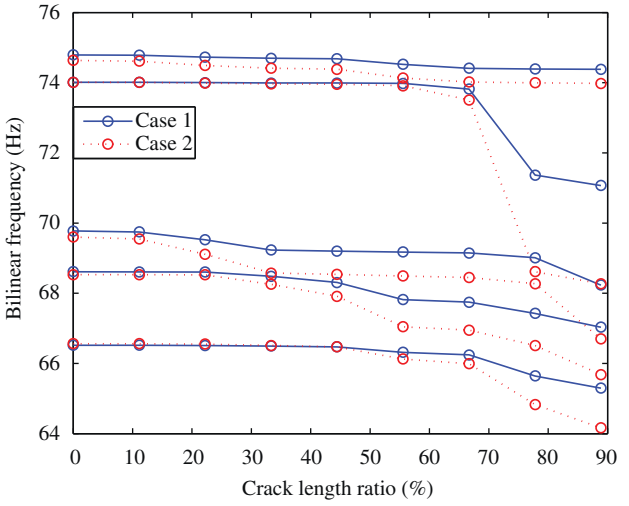

Fig. 12. Resonant frequencies predicted using BFA for the 11th–15th mode.

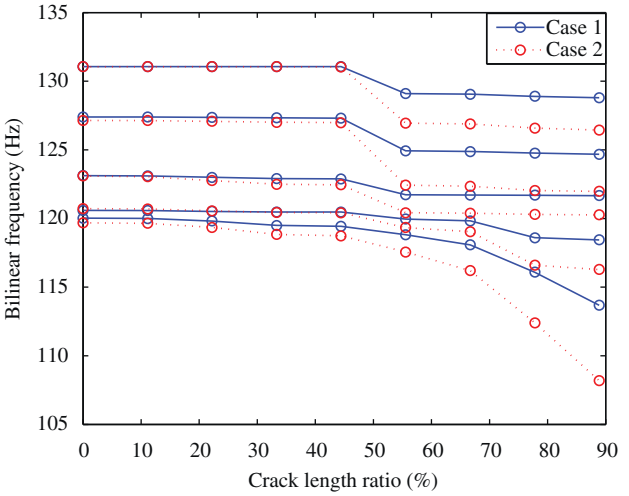

Fig. 13. Resonant frequencies predicted using BFA for the 26th–30th mode.

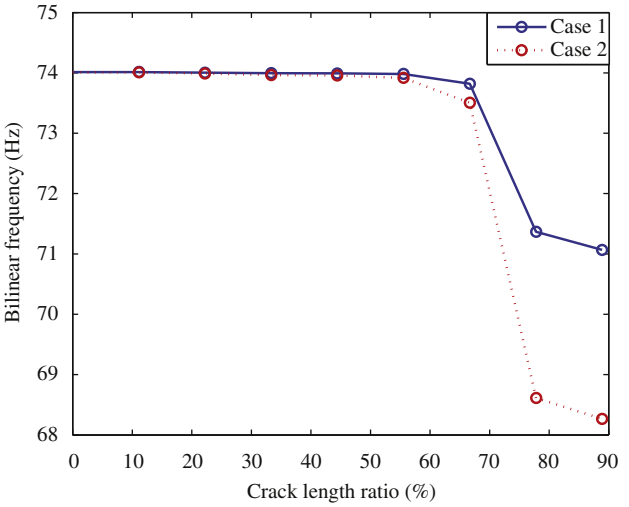

Fig. 14. Resonant frequencies predicted using BFA for the 14th mode.

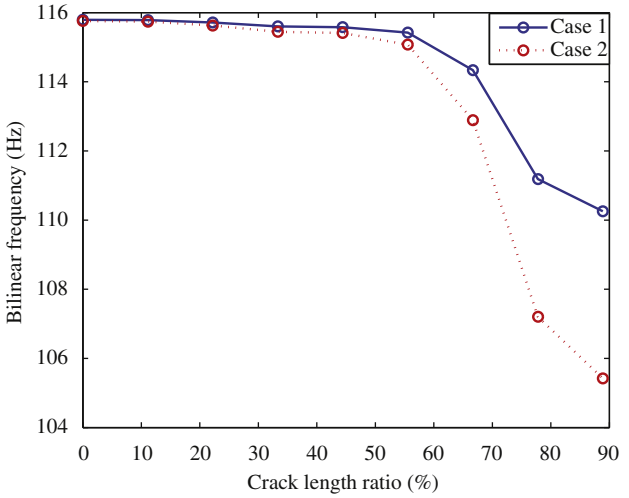

Fig. 15. Resonant frequencies predicted using BFA for the 25th mode.

the transformation matrix for each damage type. The appropriate transformation matrix to reduce the DOF of the structure has been already constructed in the initial analysis. Hence, the recalculation of the transformation matrix is not needed. That is one of the core advantages of the parametric reduced-order models (PROM) approach proposed herein.

The models developed are a viable, more efficient alternative to other component-mode-based parametric reduced-order models (PROMs). Although those models also require a reduced computation time compared to full finite element models, that computational time is still long. In particular, those models are hard to use for the analysis of huge models. These issues can be overcome by the use multiple-component parametric reduced-order models (MC-PROMs) as described herein. The key characteristic of multiple-component parametric reduced-order models (MC-PROMs) is that parametrization is applied at the component-level rather than at the system-level. As a consequence, low order approximations of the variability in the mass and stiffness matrices is effective and accurate. Note that, in general, that is not the case for system-level matrices.

To manage the geometric variations created by dents, a methodology based on component mode synthesis with static mode compensation has been developed. Furthermore, to avoid the fully nonlinear analyses, a generalized bi-linear frequency approximation has been employed for predicting resonant frequencies of complex cracked structures. The predictions of full finite element models have been shown to agree very well with the predictions obtained using (dramatically lower dimensional) reduced-order models.

The novel parametric reduced-order models (PROMs) approach provides smaller system matrices and shorter analysis and reanalysis time to predict the vibration response of complex structures. These advantages are particularly useful for optimization problems because parameter variations such as thickness variations, geometric deformations (dents), and interfaces (cracks) can easily be considered as design cases. Thus, the search for the optimal structure can be done effectively by using fast reanalyses based on parametric reduced-order models (PROMs). In contrast, conventional reduced-order modeling techniques cannot provide fast reanalyses because those reduced-order modeling are not constructed for that purpose. Instead, conventional reduced-order models reduce the size of the system matrices for *a single set of values* for the structural parameters and the geometry.

Model order reduction in general may use approximations which interfere with genuine changes in response caused by the damage. A key advantage of this work is that it is designed to address precisely this issue. Specifically, the proposed approach focuses on accurately capturing the effects of small parameter variations on the overall system response. That contrasts other existing model order reduction techniques which often turn out to be robust to such variability.

Acknowledgments

The authors gratefully acknowledge the financial support of the Automotive Research Center, a U.S. Army Center of Excellence for Modeling and Simulation of Ground Vehicles led by the University of Michigan.

Unclassified: Dist A. Approved for public release.

References

[1] W.C. Hurty, Dynamic analysis of structural systems using component modes, *AIAA Journal* 3 (4) (1965) 678–685.
[2] R.R. Craig Jr., M.C.C. Bampton, Coupling of substructures for dynamic analyses, *AIAA Journal* 6 (7) (1968) 1313–1319.

[3] S. Rubin, Improved component-mode representation for structural dynamic analysis, *AIAA Journal* 13 (8) (1975) 995–1006.
[4] R.M. Hintz, Analytical methods in component mode synthesis, *AIAA Journal* 13 (8) (1975) 1007–1016.
[5] R.R. Craig Jr., C.J. Chang, Free interface methods of structure coupling for dynamic analysis, *AIAA Journal* 14 (11) (1976) 1633–1635.
[6] M.P. Castanier, Y.C. Tan, C. Pierre, Characteristic constraint modes for component mode synthesis, *AIAA Journal* 39 (6) (2001) 1182–1187.
[7] W.H. Shyu, J.M. Gu, G.M. Hulbert, Z.-D. Ma, On the use of multiple quasi-static mode compensation sets for component mode synthesis of complex structure, *Finite Elements in Analysis and Design* 35 (2000) 119–140.
[8] L. Jezequel, S.T. Tchere, A procedure for improving component-mode representation in structural dynamic analysis, *Journal of Sound and Vibration* 144 (3) (1991) 409–419.
[9] J. Moon, D. Cho, A component mode synthesis applied to mechanisms for an investigation of vibration, *Journal of Sound and Vibration* 157 (1) (1992) 67–79.
[10] G. Masson, B.A. Brik, S. Cogan, N. Bouhaddi, Component mode synthesis (CMS) based on an enriched Ritz approach for efficient structural optimization, *Journal of Sound and Vibration* 296 (2006) 845–860.
[11] A. Shanmugam, C. Padmanabhan, A fixed-free interface component mode synthesis method for rotordynamic analysis, *Journal of Sound and Vibration* 297 (2006) 664–679.
[12] D. Kim, M. Lee, J. Jan, Substructure synthesis method for a nonlinear structure with a sliding mode condition, *Journal of Sound and Vibration* 321 (2009) 704–720.
[13] L. Hinke, F. Dohnal, B.R. Mace, T.P. Waters, N.S. Ferguson, Component mode synthesis as a frame work for uncertainty analysis, *Journal of Sound and Vibration* 324 (2009) 161–178.
[14] E. Balmès, Parametric families of reduced finite element modes: theory and application, *Mechanical Systems and Signal Processing* 10 (4) (1996) 381–394.
[15] E. Balmès, F. Ravary, D. Langlais, Uncertainty propagation in modal analysis, *Proceedings of IMAC-XXII: A Conference and Exposition on Structural Dynamics*, Dearborn, MI, IMAC-XXII-57, 2004.
[16] G. Zhang, M.P. Castanier, C. Pierre, Integration of component-based and parametric reduced-order modeling methods for probabilistic vibration analysis and design, *Proceedings of the Sixth European Conference on Structural Dynamics*, Paris, France, 2005, pp. 993–998.
[17] K. Park, G. Zhang, M.P. Castanier, C. Pierre, A component-based parametric reduced-order modeling technique and its application to probabilistic vibration analysis and design optimization, *Proceedings of ASME International Mechanical Engineering Congress and Exposition*, Chicago, IL, USA, IMECE2006-15069, 2006.
[18] K. Park, Component-based Vibration Modeling Methods for Fast Reanalyses and Design of Complex Structures, PhD Thesis, University of Michigan, 2008.
[19] S. Lim, R. Bladh, M.P. Castanier, C. Pierre, Compact, generalized component mode mistuning representation for modeling bladed disk vibration, *AIAA Journal* 45 (9) (2007) 2285–2298.
[20] S. Lim, M.P. Castanier, C. Pierre, Vibration modeling of bladed disks subject to geometric mistuning and design changes, *Proceedings of the 45th AIAA/ASME/ASCE/AHS/ASC Structures, Structural Dynamics and Material Conference*, Palm Springs, CA, AIAA 2004-1686, 2004.
[21] O. Poudou, C. Pierre, Hybrid frequency-time domain methods for the analysis of complex structural systems with dry friction damping, *Proceedings of the 44th AIAA/ASME/ASCE/AHS/ASC Structures, Structural Dynamics and Materials Conference*, Norfolk, VA, AIAA 2003-1411, 2003.
[22] O. Poudou, A new hybrid frequency-time domain method for the forced vibration of elastic structures with friction and intermittent contact, *Proceedings of the 10th International Symposium on Transport Phenomena and Dynamics of Rotating Machinery*, Honolulu, Hawaii, ISROMAC10-2004-068, 2004.
[23] S.W. Shaw, P.J. Holmes, A periodically forced piecewise linear oscillator, *Journal of Sound and Vibration* 90 (1) (1983) 129–155.
[24] M. Chati, R. Rand, S. Mukherjee, Modal analysis of a cracked beam, *Journal of Sound and Vibration* 207 (1997) 249–270.
[25] A. Saito, M.P. Castanier, C. Pierre, Estimation and veering analysis of nonlinear resonant frequencies of cracked plates, *Journal of Sound and Vibration* 326 (2009) 725–739.